3D DNS OF METHANE-AIR TURBULENT PREMIXED FLAME IN THIN REACTION ZONES WITH A DETAILED KINETIC MECHANISM

Basmil Yenerdag, Yoshitsugu Naka, Masayasu Shimura, Mamoru Tanahashi
Department of Mechanical and Aerospace Engineering
Tokyo Institute of Technology
2-12-1 Ookayama, Meguro-ku, Tokyo 152-8550, Japan
E-mail: ybasmil@navier.mes.titech.ac.jp

ABSTRACT

Three-dimensional direct numerical simulation of a stoichiometric methane–air turbulent premixed planar flame propagating in homogeneous isotropic turbulence is conducted to investigate local flame structures in thin reaction zones. The detailed kinetic mechanism (GRI-Mech 3.0) which includes 53 reactive species and 325 elementary reactions is used to represent methane–air flame. For a better understanding of the local flame structure in thin reaction zones, distributions of mass fractions of major species, heat release rate and temperature are investigated. To clarify effects of turbulence on the local flame structures in thin reaction zones, the statistical characteristics of flame elements are revealed.

INTRODUCTION

To characterize premixed flames, the ratio of turbulent intensity (u'_{rms}) to laminar burning velocity (S_L) and the ratio of length scale of turbulence (l) to nominal laminar flame thickness (δ_F) are often used. With these two parameters, classification of particular flame regimes such as the wrinkled flamelets, the corrugated flamelets, the thin reaction zones and the broken reaction zones (Peters, 2000) can be made. In practical combustors, such as gas turbine and spark ignition engines, it is considered that turbulent flame is formed in the thin or broken reaction zones. Researchers are trying to attain a deeper understanding on local flame structure of turbulent premixed flames in these particular regimes in order to develop and validate proper combustion models for engineering applications. However, due to difficulties in measurement of turbulent flames in experiments, flame structures even in the thin reaction zones have not been clarified yet.

Remarkable progress in computational technologies in recent years enabled researchers to conduct three-dimensional direct numerical simulation (DNS) of turbulent combustion with detailed chemistry. Three-dimensional DNS of hydrogen–air turbulent premixed flames with detailed chemistry have been conducted first in the world by Tanahashi *et al.* (2000, 2002) to investigate the local flame structure and the turbulence–flame interaction. Dependence of heat release rate on the three-dimensional geometrical flame elements and the tangential strain rate have been investigated. Shim *et al.* (2013) have conducted DNS of hydrogen–air premixed flames in the thin reaction zones. It has been shown that the local heat release rate in the unburned side shows 50-70% of that laminar premixed flame and found to be lower than that in the corrugated flamelets and the wrinkled flamelets (Tanahashi *et al.*, 2000, 2002; Shim *et al.*, 2011). Three-dimensional DNS of hydrogen–air premixed flame with a detailed chemistry under a pressure rising condition has been conducted for the first time in our previous study (Yenerdag *et al.*, 2015), it has been revealed that pressure change is quickly reflected in characteristics of the local flame structure.

Three-dimensional DNS of hydrocarbon flames with a detailed chemistry remains a challenge despite improvement in computational technology. Due to the high computational cost, several DNS have been done with a reduced kinetic mechanism adopting a low-Mach number approach. A complex chemistry which includes 20 species derived from GRI-Mech 1.2 mechanism and an adaptive time-dependent low-Mach number model was adopted and used by Bell *et al.* (2002, 2007, 2005). They have conducted three-dimensional DNS of lean methane–air premixed planar flames (Bell *et al.*, 2002), a laboratory scale stoichiometric Bunsen flame (Bell *et al.*, 2007) and a laboratory scale lean V-flame (Bell *et al.*, 2005). Carlsson *et al.* (2015) recently conducted three-dimensional DNS of methane–air planar premixed flames with a reduced kinetic mechanism that includes 16 species and 25 reactions. In order to develop higher accuracy of combustion models for industrial applications, it is necessary to have a better understanding of characteristics of flame elements with a more complex and detailed chemical mechanism. With this in mind, three-dimensional DNS of turbulent premixed planar flames propagating in homogeneous isotropic turbulence is conducted for the first time with GRI-Mech 3.0 kinetic mechanism (Smith *et al.*, 1999) which includes 53 reactive species and 325 elementary reactions to investigate local flame characteristics of methane–air premixed flame classified into the thin reaction zones.

DIRECT NUMERICAL SIMULATION

In this study, three-dimensional DNS of a stoichiometric methane–air turbulent premixed flame has been conducted using GRI-Mech 3.0 (Smith *et al.*, 1999) kinetic mechanism, which includes 53 reactive species and 325 elementary reactions. The DNS code developed in our previous study (Tanahashi *et al.*, 2000, 2002) is used. The Soret effect, the Dufour effect, pressure gradient diffusion, bulk viscosity and radiative heat transfer are assumed to be negli-

Table 1. Numerical parameters for DNS of methane-air turbulent premixed flames.

Re_λ	Re_l	u'_{rms}/S_L	l/δ_F	D/δ_F
37.4	144	7.14	20.1	4.64

gible. Temperature dependence of the viscosity, the thermal conductivity and the diffusion coefficients is taken into account by linking the CHEMKIN packages (Kee *et al.*, 1986, 1989) with modifications for vector/parallel computations. Figure 1 shows a schematic of the computational domain for the present DNS. The domain size is set to be 11 mm $\times$ 4.4 mm $\times$ 4.4 mm and 961 $\times$ 192 $\times$ 192 grid points are used. About 10 grid points should be contained to resolve the laminar flame thickness to calculate chemical reactions correctly, in this study, 22 grid points are within the laminar thermal flame thickness (δ_L). Navier-Stokes characteristic boundary condition (NSCBC) (Poinsot & Lele, 1992; Baum *et al.*, 1995) is used in the x direction and the periodic boundary conditions are applied in the $y-z$ directions. Governing equations are discretized by a fourth-order finite difference scheme in the x direction and a Fourier spectral method in the $y-z$ directions. Time integration is implemented by the third-order Runge-Kutta scheme. The reaction source terms in species conservation equations are advanced by the point implicit method (Brown *et al.*, 1989). The inflow boundary condition for the velocity field is given as $u_{in}(y,z,t) = (\alpha S_L, 0, 0) + u'(y,z,t)$, where, S_L is determined by preliminary one-dimensional calculations. The turbulence $u'(y,z,t)$ at the inflow boundary is given through a preliminary three-dimensional DNS of homogeneous isotropic turbulence with the spectral method and the periodic boundary conditions. α is a parameter which is determined from the ratio of the turbulent burning velocity (S_T) to the laminar burning velocity (S_L) and is set to a constant value so that the flame can stay in the computation domain for a long time. In this regard, αS_L is nearly equal to S_T. DNS is advanced at a constant 1.9 ns time step and conducted for long enough to construct statistically meaningful data.

Numerical parameters are presented in Table 1. The initial Reynolds number is $Re_l = 144$ and $Re_\lambda = 37.4$. D is the most expected diameter of the coherent fine scale eddy (Tanahashi *et al.*, 2004; Wang *et al.*, 2007) and corresponds to 8 times of the Kolmogorov length scale (η). The preheating temperature, the initial pressure and the equivalence ratio of unburned mixture are set to 950 K, 0.1 MPa and 1.0, respectively. The Karlovitz number ($Ka = (\delta_F/\eta)^2$) is 2.97. With the given parameters, the present methane-air premixed flame is classified into the thin reaction zones, as shown in Fig. 2.

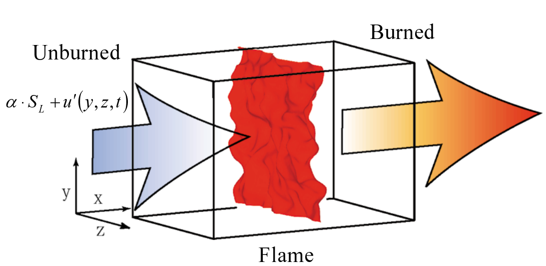

Figure 1. Schematic of computational domain.

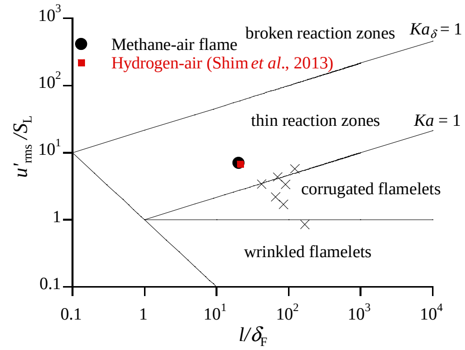

Figure 2. Turbulent combustion diagram. The cross symbols represent the previous DNS studies of H_2–air planar premixed flames (Tanahashi *et al.*, 2000, 2002; Nada *et al.*, 2004; Shim *et al.*, 2011)

LOCAL FLAME STRUCTURES

Contour surface of the heat release rate ($\Delta H/\Delta H_L$) and temperature (T) with the second invariant (Q^*) of the velocity gradient tensor (A_{ij}) are shown in Fig. 3. Q is defined by $(W_{ij}W_{ij} - S_{ij}S_{ij})/2$, where S_{ij} and W_{ij} represent the symmetric and the antisymmetric parts of A_{ij}, and is normalized by u'_{rms} and the η in the unburned side. ΔH^* is normalized by the maximum heat release rate of the corresponding laminar premixed flame (ΔH_L). The contour levels are $Q^* = 0.01$, $\Delta H^* = 1.0$ and T is set to 1944 K where the heat release rate shows the peak value in the corresponding laminar flame. As shown here, fine vortices make the flame front more complicated and increase the flame surface area.

For understanding the local flame characteristics of methane–air premixed flame in the thin reaction zones regime, the distribution of temperature (T), normalized heat

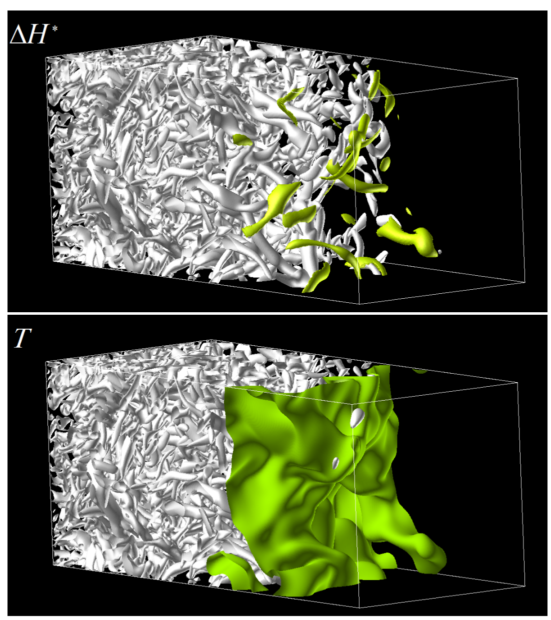

Figure 3. Contour surfaces of the heat release rate (ΔH^*) and temperature (T) with the second invariant of the velocity gradient tensor (white) ($\Delta H^* = 1.0$, $Q^* = 0.01$, T=1944 K).

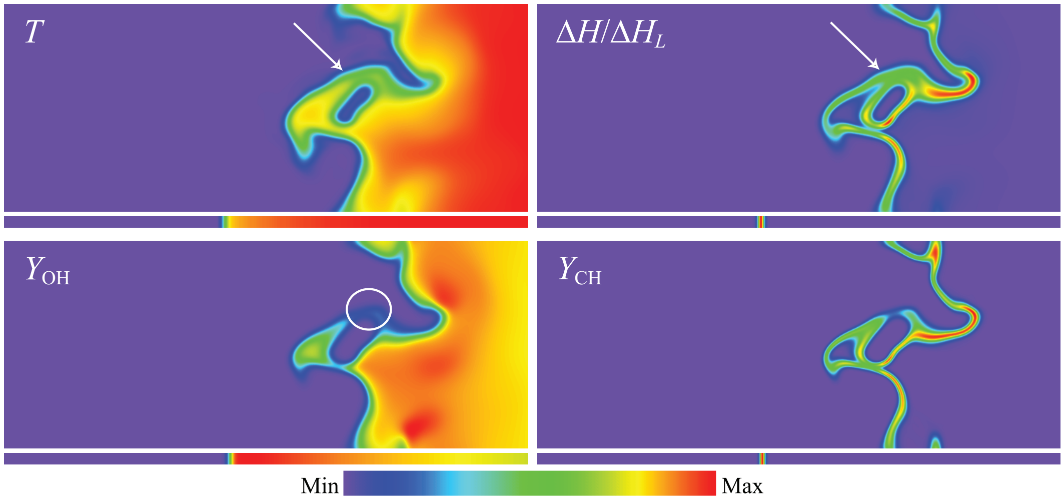

Figure 4. Distributions of Temperature (T), normalized heat release rate ($\Delta H/\Delta H_L$) and mass fractions of OH and CH on a typical plane.

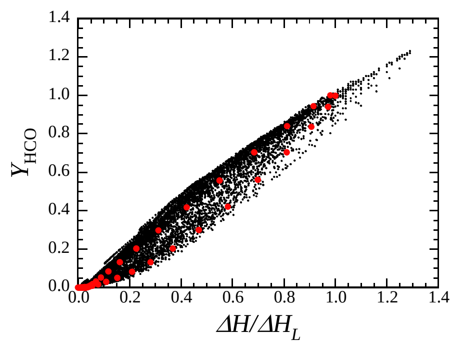

Figure 5. Scatter plots of mass fractions of HCO and local heat release rate. Red symbols correspond to laminar flame.

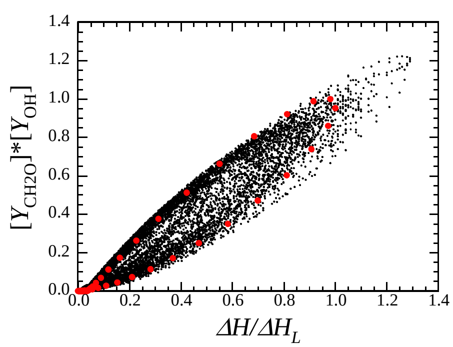

Figure 6. Scatter plots of mass fractions of CH_2O-OH and local heat release rate. Red symbols correspond to laminar flame.

release rate $\Delta H/\Delta H_L$ and mass fractions of OH and CH radicals on a typical plane are shown in Fig. 4. Here, the typical plane means an $x-z$ cross sectional plane that can represent the characteristics of each flame structure well. The corresponding laminar profile is shown in the bottom of each image. In the circled region in Fig. 4 , the concentration of OH is relatively low. However, heat release rate around 0.50-0.60ΔH_L and temperature around 1960 K can be found in the same region, which is indicated by arrows. It is difficult to measure this kind of flame structure if only OH is used to identify flame front in planar laser induced fluorescence (PLIF) measurements. These results actually reveal the limitations and drawbacks of OH, which is a commonly used flame marker in experiments. These sorts of flame structures in thin reaction zones could have significant effects on fractal analysis of the flame surface, which is one of the useful techniques to investigate characteristics of global flame structures and is often used for developments of turbulent combustion model for large eddy simulation (LES). Figure 5 shows scatter plots of normalized mass fractions of HCO versus normalized heat release rate ($\Delta H/\Delta H_L$). Values of the corresponding laminar flame are also plotted. HCO is known to be a good flame marker for methane–air premixed flames (Najm *et al.*, 1998). It can be observed that the mass fractions of HCO correlates well with heat release rate, which shows that HCO is a good flame marker as well, for the present stoichiometric methane–air premixed flame in the thin reaction zones. Recently, HCO PLIF imaging has been attempted by Zhou *et al.* (2014). However, due to low signal to noise ratio of PLIF of HCO, it was proposed that simultaneous CH_2O-OH PLIF measurement is a good flame indicator (Paul & Najm, 1998) as pixel by pixel multiplication of CH_2O and OH correlates well with local heat release rate. Figure 6 shows pixel by pixel multiplication of mass fractions of CH_2O and OH versus local heat release rate. Figure 7 shows the mass fraction distributions of CH_2O and CH_2O-OH on a typical plane. It can be seen that pixel by pixel multiplication of mass fractions of CH_2O and OH correlates well with local heat release rate for the present stoichiometric methane–air premixed flame, although the correlation of HCO between heat release rate is better, as shown in Fig. 5. Several studies on turbulent methane–air flames have used simultaneous CH-OH PLIF (Tanahashi *et al.*, 2005; Sjoholm *et al.*, 2013) and CH_2O-OH PLIF (Paul & Najm, 1998; Böckle *et al.*, 2000; Balachandran *et al.*, 2005; Roder *et al.*, 2013; Kariuki *et al.*, 2015; Gordon *et al.*, 2008; Zhou *et al.*, 2015) measurements to identify local heat release rate and flame front. Therefore, simultaneous CH-OH or CH_2O-OH PLIF measure-

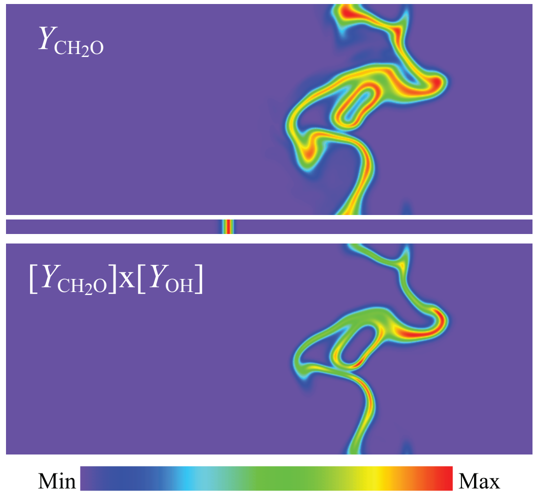

Figure 7. Distributions of mass fractions of CH_2O and CH_2O-OH on the same plane in Fig. 4.

ments may give more accurate results than single OH PLIF on the flame front measurement in thin reaction zones.

STATISTICAL CHARACTERISTICS OF LOCAL FLAME STRUCTURES

The statistical characteristics of flame elements are investigated to understand the effects of turbulence on local flame structures in the thin reaction zones. The present methane–air premixed flame is compared with stoichiometric hydrogen–air premixed flame from the previous DNS study by Shim *et al.* (2013). As shown in Fig. 2, these two cases are located in the thin reaction zones regime, and the locations of H_2–air flame and the stoichiometric CH_4–air flame are almost identical. It should be noted that the flame front is defined as surfaces with local maximum temperature gradient. Figure 8 shows the probability density function (pdf) of the local heat release rate on the flame front. The local heat release rate of the both flames are normalized by the maximum heat release rate of their corresponding laminar flame. The most expected heat release rate in the present methane flame is lower than their corresponding laminar flame, as the peaks of the pdf shows value around $0.90\Delta H_L$. For hydrogen–air flame, however, the most expected heat release rates are in the range from 1.0 to 1.1 times that of laminar flame. The maximum heat release rate reaches up to $1.4\Delta H_L$ for the methane flame, while the maximum local heat release rate shows values around $1.3\Delta H_L$ in the hydrogen case.

Figure 9 shows the pdfs of the local flame thickness (δ) for the both flames, and the local flame thickness are normalized by their corresponding laminar flame thickness δ_L. δ_L is defined by $\delta = (T_b - T_u)/(\partial T/\partial \boldsymbol{n})_{max}$, where $\boldsymbol{n}$ denotes a unit vector normal to the flame surface, and subscript u and b denote the unburned and the burned sides, respectively. It can be clearly seen that, although very thick flames can be found locally, the most expected local flame thickness for the both methane and hydrogen flames are thinner than their corresponding laminar flame. On average, however, the mean flame thickness, δ_m, increases 10% that of laminar flame for the present stoichiometric methane flame. Sankaran *et al.* (2007) have conducted three-dimensional DNS of lean methane–air Bun-

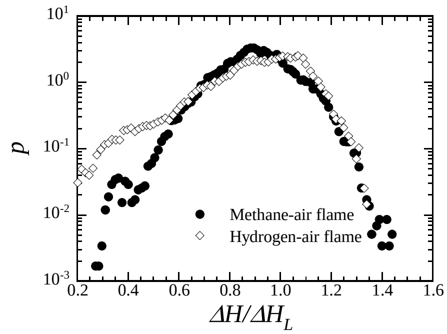

Figure 8. Probability density functions of the local heat release rate on the flame front.

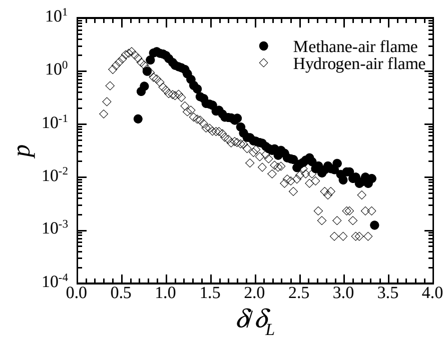

Figure 9. Probability density functions of the local flame thickness.

sen flame (ϕ = 0.7), which is classified into the thin reaction zones. They have found a thickening flame on average. Thinner flames results, however, were obtained for lean methane–air premixed flames from several experimental studies (Dinkelacker *et al.*, 1998; Soika *et al.*, 1998; Buschmann *et al.*, 1996). Recently, Tamadonfar & Gülder (2015) have conducted experiment on premixed turbulent CH_4–air flames in the thin reaction zones, they have shown that the preheat zone and the reaction zone thicknesses are thinner than the corresponding laminar flame for equivalence ratios ranging from 0.6 to 0.7, and thicker than the corresponding laminar flame for equivalence ratios ranging from 0.8 to 1.0. However, they have discussed that the reason behind flame front thickening might be due to the 2D image processing procedure when calculating flame front thickness (de Goey *et al.*, 2005). In Fig. 9, for hydrogen flame, the mean flame thickness decreases drastically, about 26% that of laminar flame.

The pdfs of the local mean curvature (k) on the flame front are shown in Fig. 10. k is normalized by the corresponding η in the unburned side. The flame elements convex toward the unburned side have negative values. The most expected k shows 0 for all cases, and the probability of positive curvature is relatively higher. This result is more pronounced in the methane flame than that in the hydrogen flame. For the both flames, the minimum curvature radius of the flame front is about twice of the Kolmogorov length scale.

Figure 11 demonstrates the pdfs of tangential strain rate (a_t) which is normalized by u'_{rms}/λ in the unburned

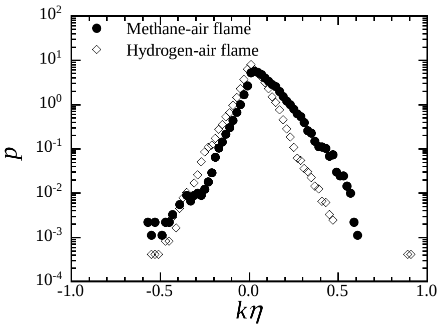

Figure 10. Probability density functions of the local mean curvature of the flame front.

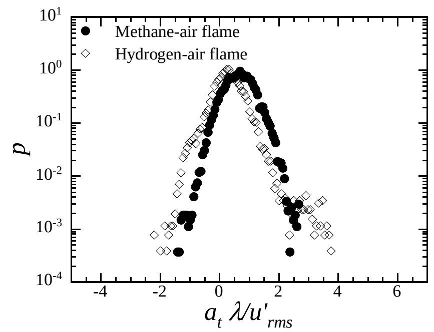

Figure 11. Probability density functions of the tangential strain rate on the flame front.

side. The positive and the negative strains represent stretch and compression, respectively. It can be seen that, all pdfs skew to the positive side and the mean a_t is positive for the both flames. This means that for methane and hydrogen flame, most of the flame elements tend to be stretched in the tangential direction. The peak of the pdf of the tangential strain rate is less than 1 Taylor time scale. The maximum strain rate tangential to the flame front in the thin reaction zones is about half of the value that is observed in the flamelet regime such as the corrugated flamelet and the wrinkled flamelet (Tanahashi *et al.*, 2000; Shim *et al.*, 2011; Yenerdag *et al.*, 2015).

CONCLUSIONS

In this study, three-dimensional DNS of methane–air turbulent premixed flame has been conducted using GRI-Mech 3.0 kinetic mechanism to investigate local flame structures of a stoichiometric methane-air premixed flame in the thin reaction zones regime.

At relatively high temperature region where heat release rate is around $0{,}60\Delta H_L$, relatively low concentrations of OH radicals are observed which could result in difficulties in OH PLIF measurement to identify flame front in experiments. These sorts of flame structures could have significant effects on fractal analysis of the flame surface, therefore, simultaneous CH-OH or CH_2O-OH PLIF measurements might give more accurate results than single OH PLIF on the characteristics of global flame structures for methane–air premixed flames classified into the thin reaction zones.

The statistical characteristics of local flame elements have been investigated and compared with hydrogen–air premixed flame in the thin reaction zones. The most expected heat release rate in methane–air premixed flames are lower than their corresponding laminar flame, as the peaks of the pdfs show value around 90% that of laminar flame. For hydrogen–air premixed flame, however, the most expected heat release rates are in the range from 1.0 to 1.1 times that of laminar flame.

The most expected local flame thickness for all flames are thinner than their corresponding laminar flame. On average, however, the mean flame thickness, δ_m, increases 10% that of laminar flame in the stoichiometric methane–air premixed flame. For hydrogen–air premixed flame, δ_m decreases around 26%.

It is revealed that in the thin reaction zones, the minimum curvature radius of the flame front is about twice of the Kolmogorov scale. The peak of the pdf of the tangential strain rate is less than 1 Taylor time scale. The maximum strain rate tangential to the flame front in the thin reaction zones is about half of the value that is observed in the flamelet regime such as the corrugated flamelet and the wrinkled flamelet. These results show that in the thin reaction zones, the effect of turbulence motion on the flame front is not as strong.

ACKNOWLEDGMENTS

This work was partly supported by Council for Science, Technology and Innovation(CSTI), Cross-ministerial Strategic Innovation Promotion Program (SIP), ”Innovative Combustion Technology” (Funding agency: JST).

REFERENCES

Balachandran, R., Ayoola, B. O., Kaminski, C. F., Dowling, A. P. & Mastorakos, E. 2005 Experimental investigation of the nonlinear response of turbulent premixed flames to imposed inlet velocity oscillations. *Combustion and Flame* **143** (1-2), 37 – 55.

Baum, M., Poinsot, T. & Thevenin, D. 1995 Accurate boundary conditions for multicomponent reactive flows. *Journal of Computational Physics* **116** (2), 247 – 261.

Bell, J. B., Day, M. S. & Grcar, J. F. 2002 Numerical simulation of premixed turbulent methane combustion. *Proceedings of the Combustion Institute* **29** (2), 1987 – 1993.

Bell, J. B., Day, M. S., Grcar, J. F., Lijewski, M. J., Driscoll, J. F. & Filatyev, S. A. 2007 Numerical simulation of a laboratory-scale turbulent slot flame. *Proceedings of the Combustion Institute* **31** (1), 1299 – 1307.

Bell, J. B., Day, M. S., Shepherd, I. G., Johnson, M. R., Cheng, R. K., Grcar, J. F., Beckner, V. E. & Lijewski, M. J. 2005 Numerical simulation of a laboratory-scale turbulent V-flame. *Proceedings of the National Academy of Sciences of the United States of America* **102** (29), 10006–10011.

Böckle, S., Kazenwadel, J., Kunzelmann, T., Shin, D., Schulz, C. & Wolfrum, J. 2000 Simultaneous single-shot laser-based imaging of formaldehyde, OH, and temperature in turbulent flames. *Proceedings of the Combustion Institute* **28** (1), 279 – 286.

Brown, P., Byrne, G. & Hindmarsh, A. 1989 Vode: A variable-coefficient ode solver. *SIAM Journal on Scientific and Statistical Computing* **10** (5), 1038–1051.

Buschmann, A., Dinkelacker, F., Schafer, T., Schafer, M. & Wolfrum, J. 1996 Measurement of the instantaneous detailed flame structure in turbulent premixed combustion. *Symposium (International) on Combustion* **26** (1), 437 – 445.

Carlsson, H., Yu, R. & Bai, X-S. 2015 Flame structure analysis for categorization of lean premixed CH_4/air and H_2/air flames at high karlovitz numbers: Direct numerical simulation studies. *Proceedings of the Combustion Institute* **35** (2), 1425 – 1432.

Dinkelacker, F., Soika, A., Most, D., Hofmann, D., Leipertz, A., Polifke, W. & Dobbeling, K. 1998 Structure of locally quenched highly turbulent lean premixed flames. *Symposium (International) on Combustion* **27** (1), 857 – 865.

de Goey, L. P. H., Plessing, T., Hermanns, R. T. E. & Peters, N. 2005 Analysis of the flame thickness of turbulent flamelets in the thin reaction zones regime. *Proceedings of the Combustion Institute* **30** (1), 859 – 866.

Gordon, R. L., Masri, A. R. & Mastorakos, E. 2008 Simultaneous Rayleigh temperature, OH- and CH_2O-LIF imaging of methane jets in a vitiated coflow. *Combustion and Flame* **155** (1-2), 181 – 195.

Kariuki, J., Dowlut, A., Yuan, R., Balachandran, R. & Mastorakos, E. 2015 Heat release imaging in turbulent premixed methane-air flames close to blow-off. *Proceedings of the Combustion Institute* **35** (2), 1443 – 1450.

Kee, R. J., Dixon-Lewis, G., Warnatz, J., Coltrin, M. E. & Miller, J. A. 1986 A fortran computer code package for the evaluation of gas-phase multicomponent transport properties. *Sandia National Laboratories* pp. Report No. SAND86–8246.

Kee, R. J., Rupley, F. M. & Miller, J. A. 1989 A fortran chemical kinetics package for the analysis of gas phase chemical kinetics. *Sandia National Laboratories* pp. Report No. SAND89–8009B.

Nada, Y., Tanahashi, M. & Miyauchi, T. 2004 Effect of turbulence characteristics on local flame structure of H_2-air premixed flames. *Journal of Turbulence* p. N16.

Najm, H. N., Paul, P. H., Mueller, C. J. & Wyckoff, P. S. 1998 On the adequacy of certain experimental observables as measurements of flame burning rate. *Combustion and Flame* **113** (3), 312 – 332.

Paul, P. H. & Najm, H. N. 1998 Planar laser-induced fluorescence imaging of flame heat release rate. *Symposium (International) on Combustion* **27** (1), 43 – 50.

Peters, N. 2000 *Turbulent Combustion*. Cambridge University Press.

Poinsot, T. J. & Lele, S. K. 1992 Boundary conditions for direct simulations of compressible viscous flows. *Journal of Computational Physics* **101** (1), 104 – 129.

Roder, M., Dreier, T. & Schulz, C. 2013 Simultaneous measurement of localized heat-release with OH/CH_2O-LIF imaging and spatially integrated OH* chemiluminescence in turbulent swirl flames. *Proceedings of the Combustion Institute* **34** (2), 3549 – 3556.

Sankaran, R., Hawkes, E. R., Chen, J. H., Lu, T. & Law, C. K. 2007 Structure of a spatially developing turbulent lean methane-air bunsen flame. *Proceedings of the Combustion Institute* **31** (1), 1291 – 1298.

Shim, Y-S., Fukushima, N., Shimura, M., Nada, Y., Tanahashi, M. & Miyauchi, T. 2013 Radical fingering in turbulent premixed flame classified into thin reaction zones. *Proceedings of the Combustion Institute* **34** (1), 1383 – 1391.

Shim, Y-S., Tanaka, S., Tanahashi, M. & Miyauchi, T. 2011 Local structure and fractal characteristics of H_2-air turbulent premixed flame. *Proceedings of the Combustion Institute* **33** (1), 1455 – 1462.

Sjoholm, J., Rosell, J., Li, B., Richter, M., Li, Z., Bai, X-S. & Alden, M. 2013 Simultaneous visualization of OH, CH, CH_2O and toluene PLIF in a methane jet flame with varying degrees of turbulence. *Proceedings of the Combustion Institute* **34** (1), 1475 – 1482.

Smith, G., Golden, D., Frenklach, M., Moriarty, N., Eiteneer, B., Goldenberg, M., Bowman, C., Hanson, R., Song, S., Gardiner, W., Lissianski, V. & Qin, Z. 1999 GRI-Mech 3.0 .

Soika, A., Dinkelacker, F. & Leipertz, A. 1998 Measurement of the resolved flame structure of turbulent premixed flames with constant reynolds number and varied stoichiometry. *Symposium (International) on Combustion* **27** (1), 785 – 792.

Tamadonfar, P. & Gülder, O. L. 2015 Experimental investigation of the inner structure of premixed turbulent methane/air flames in the thin reaction zones regime. *Combustion and Flame* **162** (1), 115 – 128.

Tanahashi, M., Fujimura, M. & Miyauchi, T. 2000 Coherent fine-scale eddies in turbulent premixed flames. *Proceedings of the Combustion Institute* **28** (1), 529 – 535.

Tanahashi, M., Kang, S.-J., Miyamoto, T., Shiokawa, S. & Miyauchi, T. 2004 Scaling law of fine scale eddies in turbulent channel flows up to Re_τ=800. *International Journal of Heat and Fluid Flow* **25** (3), 331 – 340.

Tanahashi, M., Murakami, S., Choi, G-M., Fukuchi, Y. & Miyauchi, T. 2005 Simultaneous CH-OH PLIF and stereoscopic PIV measurements of turbulent premixed flames. *Proceedings of the Combustion Institute* **30** (1), 1665 – 1672.

Tanahashi, M., Nada, Y., Ito, Y. & Miauchi, T. 2002 Local flame structure in the well-stirred reactor regime. *Proceedings of the Combustion Institute* **29** (2), 2041 – 2049.

Wang, Y., Tanahashi, M. & Miyauchi, T. 2007 Coherent fine scale eddies in turbulence transition of spatially-developing mixing layer. *International Journal of Heat and Fluid Flow* **28** (6), 1280 – 1290.

Yenerdag, B., Fukushima, N., Shimura, M., Tanahashi, M. & Miyauchi, T. 2015 Turbulence-flame interaction and fractal characteristics of H_2-air premixed flame under pressure rising condition. *Proceedings of the Combustion Institute* **35** (2), 1277–1285.

Zhou, B., Brackmann, C., Li, Z., Aldén, M. & Bai, X-S. 2015 Simultaneous multi-species and temperature visualization of premixed flames in the distributed reaction zone regime. *Proceedings of the Combustion Institute* **35** (2), 1409 – 1416.

Zhou, B., Kiefer, J., Zetterberg, J., Li, Z. & Alden, M. 2014 Strategy for PLIF single-shot HCO imaging in turbulent methane/air flames. *Combustion and Flame* **161** (6), 1566 – 1574.